Digest Journal of Nanomaterials and Biostructures Vol. 6, No 4, October-December 2011, p. 1877-1886

STRUCTURAL, OPTICAL AND ELECTRONIC PROPERTIES OF $In_{1-x}Y_xN$ THIN FILMS

C.N.ZOITA, M.BRAIC[*], V.BRAIC
National Institute for Optoelectronics, 409 Atomistilor, 077125, Magurele, Romania

The study of IIIA-IIIB-V type thin films has recently been receiving a great deal of attention as possible solutions to optimize and to further engineer the electronic, optical and structural properties of optoelectronic materials. In this work we studied the influence of yttrium addition to InN films, in connection with YN band-gap, and explored the possibility of tuning the optical and electronic properties of $In_{1-x}Y_xN$ thin films for low concentration of yttrium. Reactive sputtering method was used in this work to grow thin films of $In_{1-x}Y_xN$ with low yttrium concentrations, $0 \leq x \leq 0.094$, as well as of a pure YN ($x = 1$), on fused quartz substrates at 500 ^oC. At low Y contents ($0 \leq x < 0.1$), the wurtzite structure of InN was preserved. $In_{1-x}Y_xN$ films exhibited the specific alloy-type behavior of the compound - with linear variation of the lattice constants, optical band-gap, carrier mobility and surface roughness with the Y content. Encouraging evidences for tuning the electron concentration in $In_{1-x}Y_xN$ thin films were observed. YN films were obtained in a rock-salt structure, with an indirect band-gap of about 0.498 eV, which represent, up to our knowledge, the first experimental evidence of the existence of the indirect optical band-gap in c-YN.

(Received November 23, 2011; accepted December 5, 2011)

Keywords: $In_{1-x}Y_xN$, thin films, magnetron sputtering

1. Introduction

Group III nitrides (GaN, InN and AlN and their alloys) have been the subject of extensive research in the last decades due to their technological applications especially those based on band-gap engineering [1]. Recently, there were reported studies about using different IIIA-V and IIIB-V group nitrides, in order to optimize and to further engineer their electronic, optical and structural properties as optoelectronic materials [1-6]. Band-gap engineering has been successfully demonstrated in a lot of semiconductors, including ScGaN [2-5], and similar behavior is anticipated in the (Sc,In)N system [6-9].

During the years, YN has received little attention. There are only some theoretical but very few experimental reports. The structure of YN is either face-centered cubic (fcc), or hexagonal closed packed (hcp), the cubic one having the lowest energy formation [10]. It was predicted that YN can be crystallized either in a cubic or in a hexagonal structure; however up-to-date only YN thin films with fcc structure (c-YN) were experimentally observed [6, 14-15], even if detailed calculations were done for the hexagonal structure (*w*-YN) [16]. For c-YN only direct optical transitions were experimentally reported (at 1.5 eV in [14] and at 2.3 eV in [6]), while spectroscopic ellipsometry characterization suggested that c-YN has no direct band-gap less than 2.6 eV [15]. The theoretical prediction affirms that *w*-YN is an indirect semiconductor with an indirect band-gap of about 2 eV [16]. No measurement of the YN indirect band-gap has been reported so far. The potential applications of YN in micro and optoelectronics promote the interest in deposition techniques that can optimize the structural, optical and electron transport properties

[*]Corresponding author: mariana_braic@inoe.ro

[17 - 18]. Due to the small difference in lattices constants between InN and YN, of about 2%, we propose in this paper to explore the properties of the $In_{1-x}Y_xN$ thin films.

Pure InN, with wurtzite ground state structure, has applications in its own right. It is highly desirable for applications in high speed and high power electronic devices and various types of sensors [19-20] because of its unique set of properties, such as high electron mobility and high saturation velocity [21-22]. InN also has promising applications for terahertz devices [23.].

However, the growth of high quality InN films is still difficult mainly due to its low dissociation temperature of about 600 °C, the absence of lattice and thermal matched substrates and due to impurity incorporation problem, especially of oxygen [24]. InN films were found to be always unintentionally n-type doped, usually in the range of 10^{18}-10^{21}cm^{-3} [25] and the source of this conductivity is still unknown, being under debate [24 - 26]. Various theoretical and experimental assessments, suggest various sources for the high electron carrier concentration of InN: i) oxygen atoms on nitrogen sites [27]; ii) hydrogen incorporation [24, 28] and iii) nitrogen vacancies [29]. In present efforts are made to understand and control the optical and electrical properties of InN [30 - 32].

The aim of this work is to study the influence of yttrium addition to InN films, in connection with YN band-gap, and to explore the possibility of tuning the optical and electronic properties of of $In_{1-x}Y_xN$ thin films for low concentration of yttrium, up to 9.4 at.%.

2. Experimental procedure

2.1. Deposition of $In_{1-x}Y_xN$ films

$In_{1-x}Y_xN$ films were deposited on fused quartz substrates by reactive magnetron sputtering of a In and Y targets (99.99% purity, 50 mm diameter, 5 mm thick) in a discharge atmosphere of pure N_2 (99.998%), using a con-focal sputtering AJA ATC-ORION system. A 13.56 MHz AJA-Seren RF generator delivered 100 W to the In cathode, while a DC AJA-Seren power supply powered the Y target at different power values. The substrates were placed on a rotating holder, at 170 mm away from the sputtering target and directly facing it. The substrates were ultrasonically cleaned in acetone and isopropyl alcohol and then located in the vacuum chamber. Plasma etching of thus pre-cleaned substrates and of the In and Y targets followed for 10 minutes at 300 W power in a 0.27 Pa Ar atmosphere. The deposition chamber was evacuated down to 7 x 10^{-6} Pa prior to film deposition. The N_2 gas mass flow rate and the deposition pressure were held constant at 5 sccm and 0.27 Pa, respectively. The substrate temperature (T_S) was measured with a backside non-contact thermocouple and was maintained constant at 500 ^oC with an accuracy of ± 5 ^oC. Six sets of samples were deposited at different sputtering power values fed on Y cathode. The duration of all depositions was 60 minutes. The deposition rate was calculated as the ratio between the measured film thickness and the deposition time. The table 1 displays the labels of the $In_{1-x}Y_xN$ samples along with the corresponding deposition parameters.

Table 1 Growth parameters for $In_{1-x}Y_xN$ thin films deposition by magnetron reactive sputtering (power fed on In and Y cathodes, film thickness t, deposition rate D_R), and yttrium content of the film $x = N_Y/(N_Y + N_{In})$.

Sample	P_{In} (W)	P_Y (W)	*t* (nm)	D_R (nm/min)	*x*
S1	100	0	144.6	2.4	0
S2	100	7	154.8	2.6	0.016
S3	100	13	159.6	2.7	0.032
S4	100	25	164.4	2.7	0.062
S5	100	30	168.0	2.8	0.094
S6	0	300	118.8	0.7	1

2.2. Films' characterization

The crystallographic structure of the films was investigated using a Bruker D8 ADVANCE X-ray diffraction (XRD) system equipped with a copper target X-ray tube and a scintillation detector. A parallel beam geometry at grazing incidence $\alpha = 3°$ in $2\theta/\ \theta$ scan mode was employed, with a Göbel mirror in the incident beam. An asymmetric channel cut monochromator installed after the mirror provided a strictly monochromatic $CuK_{\alpha 1}$ primary X-ray beam.

The thickness of the films (t) was determined with a Dektak 150 Veeco surface profiler from a step height in a masked area on the substrate.

The surface roughness and morphology were investigated with an INNOVA Veeco atomic force microscope operating in the tapping mode.

Optical transmittance (T) and reflectance (R) spectra have been recorded over the 190-2500 nm spectral range (1 nm and 8 nm resolution on respectively UV-VIS and NIR ranges) by a double beam JASCO V670 spectrophotometer equipped an integrating sphere. The absorption coefficient, α, was deduced from the $\alpha t = \ln((1- R)/T)$ relationship.

X-ray photoelectron spectroscopy (XPS) method was used to determine the chemical bonds in the films. XPS spectra were taken with a VG ESCA 3MKII spectrometer, using Al K_{α} radiation (1486.6eV). A 2 keV Ar^{+} ion beam was used for sputter etching of the specimens for 2 minutes.

The films' electrical properties were determined at room temperature by Ecopia HMS-3000 Hall measurement system, using a Van der Pauw geometry, in a 0.55 T magnetic field. The film contacts were routinely confirmed to be ohmic by noting a linear current response to a dc voltage sweep.

3. Results and discussions

Table 1 presents the yttrium content of the films, $x = N_Y/(N_Y + N_{In})$, where N_Y and N_{In} are the number of Y and In atoms within a given volume respectively, obtained from XPS data analysis. Depending on the power fed on Y target, yttrium was incorporated into the films up to 9.4% relative to indium content. The oxygen content of the films was of about 10 %, probably due to samples' manipulation in open atmosphere, and in between the deposition and characterization equipments. It has been proposed that the oxygen is incorporated in the columnar polycrystalline InN thin films, as usually obtained by sputter deposition, due to the film exposure at ambient atmosphere. We can conclude that an amorphous layer comprising both oxyde and oxynitride species is formed at the grain boundaries [33]. In this case, the oxygen content in these films should be related with the size of the grains. In the case of oxygen containing substrates, such as fused quartz, the observed oxygen contamination of the film may be also due to oxygen diffusion from the substrate during film growth at $T_S > 300\ ^0C$ [34].

AFM studies showed that the as-grown $In_{1-x}Y_xN$ films had a relatively rough surface. The surface roughness increased linearly with increasing Y concentration (Fig. 1). This effect may be attributed to decreasing of the homologous temperature of the deposited material (T_g/T_m, where T_g is the growth temperature and T_m is the melting point of the material) due to the higher melting point of YN (~ 2500 °C) [35] as compared to InN (1100 ºC) [36]. Even if the above melting temperatures are true for the atmospheric pressure, at the low pressures specific for the deposition system, it is preserved a difference between the melting temperatures of the two materials.

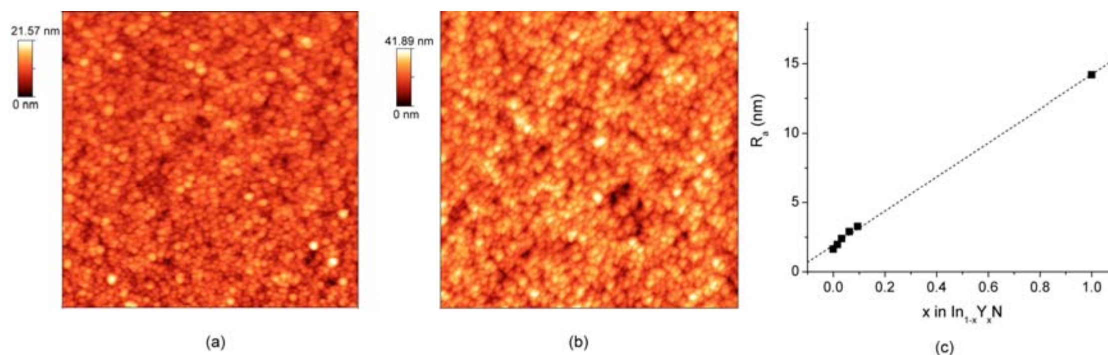

Fig. 1 3 x 3 μm² AFM images of (a) S1 and (b) S5 samples. (c) The variation of the surface roughness, Ra, of $In_{1-x}Y_xN$ films calculated from parabola-flattened 3 x 3 μm² AFM scans with increasing film Y content. The dotted line represents the least-squares linear data fit

Fig. 2 presents the In 3*d*, Y 3d, N 1*s*, and O 1*s* XPS core-level spectra recorded from the S4 sample. In 3d spectrum (Fig. 2a) contains In $3d_{5/2}$ and In $3d_{3/2}$ spin-orbit doublet, which are separated by 7.56 eV with the intensity ratio of 1.63, in good agreement with Ref. [37]. The spectral feature of In $3d_{5/2}$ can be deconvoluted into two peaks at about 444.48 and 445.59 eV. The peak at about 444.48 eV can be assigned to the electron binding energy (BE) of In in InN [38], while the higher energy peak at about 445.59 eV can be attributed to In-O bonding [39]. In Fig. 2b the deconvolution of Y 3d core level spectra of S4 sample indicates peaks with binding energies around 158.58 eV and 160.51 eV which corresponding to the Y $3d_{5/2}$ and Y$3d_{3/2}$ spin–orbit coupling states of Y-O bonding states of Y_2O_3 [40]. The lower energy group of peaks identified at about 156.74 eV and 158.49 eV are in closed proximity of the 156.64 eV and 158.68 eV peaks, respectively identified in the Y_{3d} deconvoluted spectrum of YN sample (Fig. 2e). They can be assigned to the Y $3d_{3/2}$ and Y $3d_{5/2}$ states of Y bonded in YN, in good agreement with ref [15] which suggested a value of 156.6 eV for the binding energies of Y $3d_{3/2}$ state of YN.

The feature at 396.7 eV dominates the XPS spectra in the BE region of N1s. It is interpreted as N atoms bounded to metallic atoms - In and Y [15, 41]. The additional peak observed at BE 397.7 eV is probably originating from the N–O bonds, due to oxynitrides formation [42]. The O1*s* core-level spectra (Fig 1d) suggest the presence of physi-sorbed oxygen on the films' surface - the peak at about 532.4 eV [43]. During Ar^+ etching this peak diminishes and the peak at 530.3 eV can be identified. It can be attributed to the sum of the contributions of O-In and O-Y bonding states of In_2O_3 at BE 530.4 eV in [44] and 529.5 eV in Y_2O_3 [45], respectively. From XPS data it may be concluded that at the surface of the film, a fraction of yttrium is bonded to oxygen in the form of Y_2O_3, due to the higher affinity of yttrium to oxygen (ΔH_f^0 (Y_2O_3) = 1932.8 kJ/mol. [46]), as compared to indium affinity to it (ΔH_f^0 (In_2O_3) = 923.5 kJ/mol. [47]).

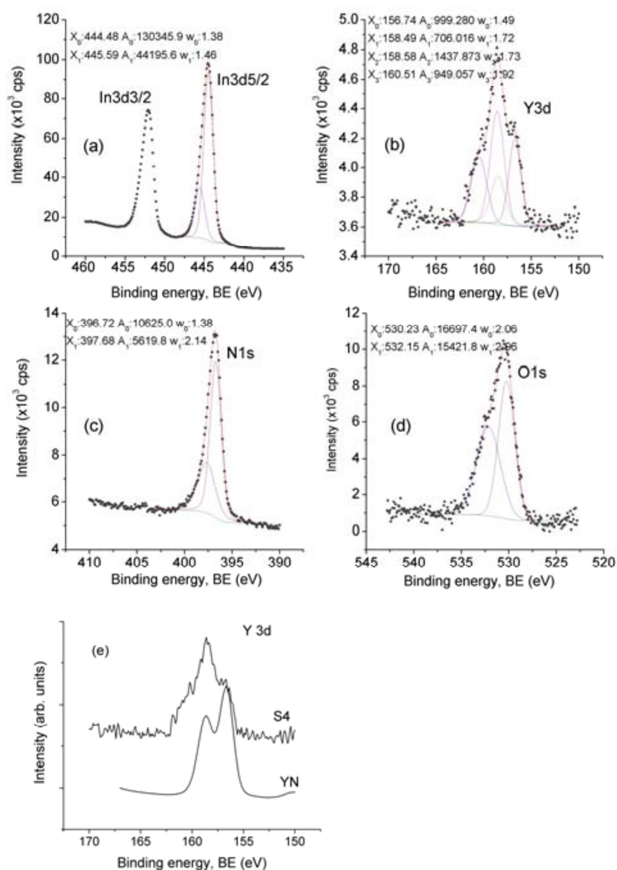

Fig. 2 (a) In 3d, (b) Y 3d, (c) N 1s and (d) O1s XPS spectra of $In_{0.94}Y_{0.06}N$ film.
(e) Comparison of Y 3d photoelectron spectra of S4 and S6 (YN) samples.

The 2θ/θ X-ray diffraction patterns of the $In_{1-x}Y_xN$ samples are displayed in the logarithmic scale in Fig. 3a. The diffraction peaks identified in the recorded spectra of the S1 (InN) sample around 31.3°, 57.0° and 65.3° are assigned to the hexagonal wurtzite InN phase (α-InN) [48], corresponding to (002), (103) and (004) planes respectively. No traces of crystalline cubic InN or indium oxyde phases could be identified. The film is polycrystalline - as suggested by the presence of (103) diffraction maximum - and exhibits a preferred (002) basal orientation, meaning that InN thin films are highly textured in the [001] direction, with the c-axis perpendicular to the surface of the substrate. This characteristic is preserved with addition of yttrium to the InN material (S2 - S5 samples). The (103) peak is slightly intensified with increasing x, demonstrating the disturbed preferential orientation. Also, as compared to InN sample, no additional diffraction lines could be identified. Because XPS data demonstrated the presence of additional oxyde and oxynitride phases, it can be assumed that these phases are in amorphous state.

Fig. 3b shows the diffraction patterns of S6 (YN) sample. Only a weak diffraction line can be identified at about 31.6° corresponding to *w*-YN (111), in agreement with the reference data (JCPDS 035-0779). YN(111) is located in the closed proximity of the InN (002) maximum identified at about 31.3°, meaning that a possible InN - YN phase separation in the $In_{1-x}Y_xN$ compound can be difficult to be accurately identified, if exists. Most probably, for small x values, Y is positioned within the *w*-InN lattice and is not forming a separate sublattice.

It can be concluded that for low yttrium content in the films ($x < 0.1$) $In_{1-x}Y_xN$ presents a polycrystalline single phase with wurtzite structure, even if the ground state phase of YN is a rock-salt one, as results from *ab initio* calculations [10]. The transition of the crystallographic structure

from a wurtzitic to a fcc one is expected to occur at higher *x* values, similar with the reported phase transition of $Sc_{1-x}Ga_xN$ alloy, when Sc content progressively increased [4].

The position of $In_{1-x}Y_xN$ (002) peak is found to shift towards lower 2θ values as *x* increases. That means that the c-lattice spacing (<c>) is elongated due to yttrium incorporation into the films. Fig. 3c shows the dependence of <c> versus film composition. The c-lattice parameter was calculated using the Bragg's law and a Lorrentian peak fitting procedure. Extrapolating the straight line fit of that data towards $x = 1$, it results a value of <c> = 5.91 Å for a hypothetical YN in hexagonal (wurtzite) phase (*w*-YN). This value is slightly lower, but still in good agreement, with the theoretical values of 5.95 – 6.04 Å [10, 16, 49] predicted for *w*-YN, being shown in Fig. 3c for completitude. The agreement between the theoretical and experimental data confirms the wurtzite structure for in-rich $In_{1-x}Y_xN$ films ($x < 0.1$). Also, the linear variation of $In_{1-x}Y_xN$ (002) peak position towards the position of *w*-YN (002) maximum demonstrates the solubility of Y in InN, within the explored concentrations interval. However, our value obtained for <c> lattice parameter in *w*-YN seems to be slightly underestimated, compared to the theoretical predictions. This could be related to the incertainties related to either the extrapolation to large *x* values of the experimental data obtained for $x < 0.1$, or to the inherent incertainity on the content of metals properly incorporated within the $In_{1-x}Y_xN$ lattice, as not all the metallic atoms are positioned into it. Amorphous oxyde and oxynitride phases are most probably present at the grain boundary, at the film' surface, and at the films-substrate interface, as fused quartz - an oxygen rich material, was used as substrate. Anyway, the ratio between the metals incorporated within the lattice and the ones contributing to the amorphous phase might change as *x* increases.

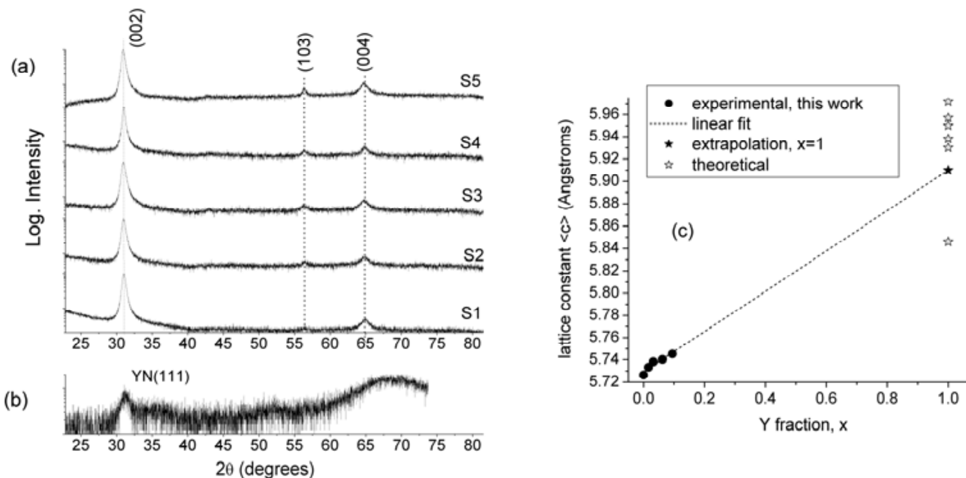

Fig. 3 XRD patterns of (a) $In_{1-x}Y_xN$, $x < 0.1$ and (b) YN samples. (c) Wurtzite lattice parameter, <c>, of $In_{1-x}Y_xN$ versus film composition. Least-squares linear fit to the data extrapolated to x = 1 finds $\langle c\rangle_{(w\text{-}YN)}$ = 5.91 Å. Theoretical values of $\langle c\rangle_{(w\text{-}YN)}$ are shown for comparisson: 5.846 Å, 5.957 Å, 5.938 Å, 6.041 Å [16], 5.972 Å [49], and 5.956 Å [10].

Fig. 4 shows a slight blue-shift of the direct optical absorption edge (E_g) with increasing yttrium content. The optical band-gap was determined from the energy axis intercept of the straight line tangent to the curve $(\alpha h\nu)^n = f(h\nu)$ near its inflection point, considering n = 2 for the direct optical transition and n = ½ for the indirect one [50]. The E_g values plotted versus *x* in Fig 4, are indicating a linear dependence of the optical band-gap with the yttrium content in the films. The straight line fit of E_g versus *x* data prolonged to $x = 1$ generates a hypothetical value of 2.38 eV for the direct optical band-gap of *w*-YN. This is in good agreement with theoretical findings which established that *w*-YN is an indirect semiconductor which should exhibit an indirect band-gap with a value close to 2 eV [16]. It seems that the evolution of the optical band-gap in $In_{1-x}Y_xN$ films is determined by the alloying process of the two components. In the deposited films there were not evidenced indirect optical transitions. We used this opportunity to find indirect transitions in the YN films (samples S6). We found strong evidence of an indirect band-gap in c-YN at about 0.49 eV (Fig. 5) in good agreement with the theoretical prediction of 0.54 eV [13]. Up to our

knowledge this finding seems to be the first experimental evidence of the existence of the indirect band-gap in c-YN.

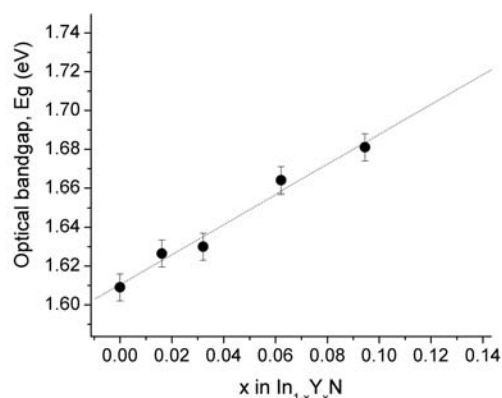

Fig. 4 Optical band-gap in $In_{1-x}Y_xN$ films blueshifts as x increases ($0 < x < 0.1$)

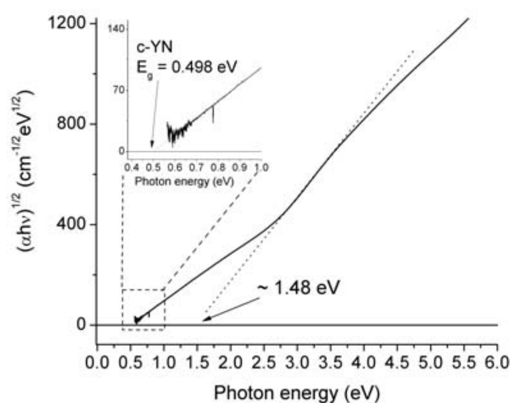

Fig. 5 Evidence of the indirect band-gap in c-YN, at about 0.49 eV; the other transition observed at 1.48 eV, is probably due to oxygen contamination of the YN sample

Hall effect measurements indicated that all the deposited films are n-type unintentionally doped, exhibiting high carrier concentrations, in the range of 10^{20} cm^{-3}. As previously discussed, among the possible causes of n-type doping of InN are nitrogen vacancies and unintentional impurities, such as oxygen. Also, the conditions at the film's surface can exert a large influence on defects and impurities incorporation, especially in polycrystalline films, due to their inherent high surface area. Previously were presented evidences for the presence of oxygen impurities in our films and for an increased surface roughness with increasing yttrium content. However, it was observed a decreased concentration of free electrons at yttrium addition to the films (Fig 6a). One possible explanation may come from the yttrium high affinity for oxygen of, as discussed above. XPS and XRD data suggest that an yttria amorphous secondary phase should exist. The oxygen bonded in an Y_2O_3 secondary phase does not act as electrons donor, instead it decreases the concentration of donor oxygen impurity leading to the decrease of the free electrons concentration. This fact is similar with the observation of role played by In_2O_3 phase in InN films previously reported [51], where, during intentional oxidation of InN, the free electron concentration was limited by the onset of In_2O_3 phase.

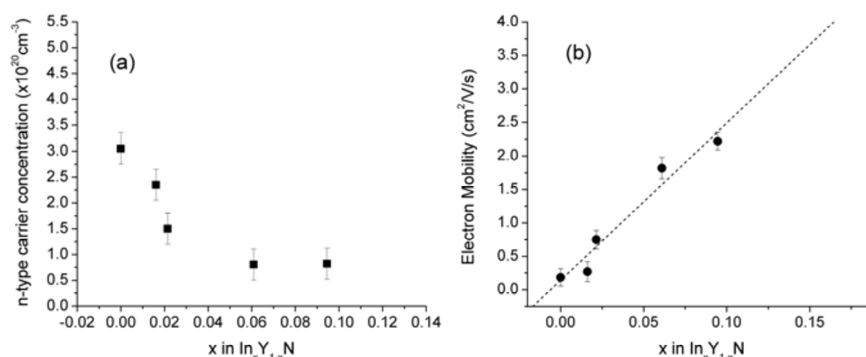

Fig. 6. Hall probe measurements of (a) electron mobility and (b) free electron concentration in $In_{1-x}Y_xN$ films.

The dependence on film composition, x, of the n-type carrier mobility (μ) is plotted in Fig. 6(b). The electron mobility μ was found to increase with increasing yttrium content in the $In_{1-x}Y_xN$ films. By extrapolation of the straight line fit of the experimental data to $x = 1$ we could derive a value of 23.5 cm^2/V/s for the electrons' mobility in YN. This value is comparable with the μ values obtained in Ref [18] for the YN films with rock-salt structure grown by MBE. Even if that sample was considered as far from being optimized, very high values for YN mobility are speculated due to observed mobility power laws [18]. We mention that the Hall measurements could not be performed on our YN sample due to the apparent imperfect electrical contacts, probably due to fast corrosion of film surface in ambient air or due to isolated columnar structure of the film.

4. Conclusions

To summarize, we have shown that despite of the different ground state crystal structures of InN and YN, at low value of Y concentrations in InN ($x < 0.1$), the $In_{1-x}Y_xN$ system has a wurtzite structure and presents an alloy-type behavior of its structural, optical and electrical properties. With increasing x we found linear increased surface roughness of the films due to increased melting point of the material, linear elongation of the <c> lattice constant, linear blue-shift of the optical band-gap, and apparently the linear increase of the n-type carrier mobility, concomitant with a decrease of carrier concentration. These are evidences of Y solubility in InN within the explored concentrations interval. Among the investigated thin films' properties, the evolution of electrical parameters are the most interesting, encouraging further work for testing the possibility of tuning the electron concentration of InN, using oxygen free substrates. YN films, obtained at $x = 1$, presented a rock-salt structure, with an indirect band-gap of about 0.498 eV. Up to our knowledge it seems to be the first experimental evidence of the existence of the indirect optical band-gap in c-YN.

Acknowledgements

This work was supported by a grant of the Romanian National Authority for Scientific Research, CNMP under the Project MINNA 72-162.

References

[1] S. Strite and H. Morkoc, J. Vac. Sci. Technol. B **10**, 1237 (1992).
[2] M.E. Little, M.E. Kordesch, Appl. Phys. Lett. **78**, 2891 (2001).
[3] M. A. Moram, Y. Zhang, T. B. Joyce, D. Holec, P. R. Chalker, P. H. Mayrhofer, M. J. Kappers, C. J. Humphreys, J. Appl. Phys. **106**, 113533 (2009).

[4] C. Constantin, H. Al-Brithen, M.B. Haider, D. Ingram, A.R. Smith, Phys. Rev. B, 193309 (2004).
[5] C. Constantin, M.B. Haider, D. Ingram, A.R. Smith, N. Sandler, K. Sun, P. Ordejon, J. Appl. Phys. **98**, 123501 (2005)
[6] J.M. Gregoire, S.D. Kirby, M.E. Turk, R.B. van Dover, Thin Solid Films **517**, 1607 (2009)
[7] V. Ranjan, L. Bellaiche, E. Walter, Phys. Rev. Lett. **90**, 257602 (2003).
[8] V. Ranjan, S. Bin-Omran, L. Bellaiche, A. Alsaad, Phys. Rev. B **71**, 195302 (2005).
[9] V. Ranjan, S. Bin-Omran, D. Sichuga, R. Nichols, L. Bellaiche, A. Alsaad, Phys. Rev. B **72**, 085315 (2005).
[10] S. Zerroug · F. Ali Sahraoui · N. Bouarissa, Appl Phys A **97,** 345 (2009)
[11] B. Saha, T. D. Sands, U. V. Waghmare, J. Appl. Phys. **109**, 073720 (2011).
[12] C. Stampfl, W. Mannstadt, R. Asahi, A. J. Freeman, Phys. Rev. B **63**, 155106 (2001).
[13] L. Tie-Yu and H. Mei-Chun, Chin. Phys. **16**, 62 (2007).
[14] J. P. Dismukes, W. M. Yim, J. J. Tietjem, R. E. Novak, RCA Rev. **31**, 680 (1970).
[15] W. De La Cruz, J. A. Diaz, L. Mancera, N. Takeuchi, and G. Soto, J. Phys. Chem. Solids **64**, 2273 (2003).
[16] Y. Cherchab, B. Amrani, N. Sekkal, M. Ghezalia, K. Talbi Physica E **40**, 606 (2008).
[17] E. I. Isaev, S. I. Simak, I. A. Abrikosov, R. Ahuja, Yu. Kh. Vekilov, M. I. Katsnelson, A. I. Lichtenstein, B. Johansson, J. Appl. Phys. **101**, 123519 (2007)
[18] J. M. Gregoire, S. D. Kirby, George E. Scopelianos, F. H. Lee, R. Bruce van Dover, J. Appl. Phys. **104**, 074913 (2008)
[19] H. Morkoc, J. Vac. Sci. Technol. B **10**, 1237 (1992).
[20]A. G. Bhuiyan, A. Hashimoto, A. Yamamoto, J. Appl.Phys. **94**, 2779 (2003).
[a34 -21]S. K. O'Leary, B. E. Foutz, M. S. Shur, U. V. Bhapkar, L. F. Eastman, J. Appl. Phys. **83**, 826 (1998).
[22] J. Wu, W. Walukiewicz, K. M. Yu, W. Shan, J. W. Ager, E. E. Haller, H. Lu, W. J. Schaff , W. K. Metzger, S. Kurtz, J. Appl. Phys. **94**, 6477 (2003).
[23] G. D. Chern, E. D. Readinger, H. Shen, M. Wraback, C. S. Gallinat, G. Koblmuller, J. S. Speck, Appl. Phys. Lett. **89**, 141115 (2006).
[24] C. G. Van de Walle, J. L. Lyons, and A. Janotti, Phys. Status Solidi A **207**(5), 1024 (2010).
[25] H. Lu, W. J. Schaff, L. Eastman, and C. E. Stutz, Appl. Phys. Lett. **82**, 1736 (2003).
[26] R. E. Jones, S. X. Li, L. Hsu, K. M. Yu, W. Walukiewicz, Z. Lilienthal-Weber, J. W. Ager, E. E. Haller, H. Lu, W. J. Schaff, Physica B **376**, 436 (2006).
[27] C. S. Gallinat, G. Koblmu¨ller, J. S. Speck, Appl. Phys. Lett. **95**, 022103 (2009).
[28] S. Limpijumnong and C. G. Van de Walle, Phys. Status Solidi B **228**, 303 (2001).
[29] T. L. Tansley and R. J. Egan, Phys. Rev. B **45**, 10942 (1992)
[30] R. E. Jones, K. M. Yu, S. X. Li, W. Walukiewicz, J.W. Ager, E. E. Haller, H. Lu, W. J. Schaff, Phys. Rev. Lett. **96**, 125505 (2006).
[31] R. E. Jones, S. X. Li, and E. E. Haller, H. C. M. van Genuchten, K. M. Yu, J. W. Ager, Z. Liliental-Weber, W. Walukiewicz, H. Lu, W. J. Schaff, Appl. Phys. Lett. **90**, 162103 (2007)
[32] J. Wu, J. Appl. Phys. **106**, 011101 (2009).
[33] K.S.A. Butcher, T.L. Tansley, Superlattice Microstruct. **38**, 1 (2005).
[34] T. S. Yeh, J. M. Wu, W. H. Lan, Thin Solid Films **517**, 3204 (2009)
[35] C. P. Kempter, N. H. Krikorian, and J. C. McGuire, J. Phys. Chem. **61**, 1237 (1957).
[36] J.B. MacChesney, P.M. Bridenbaugh, P.B. O'Connor, Mater. Res. Bull. **5**, 783 (1970).
[37] J.F. Moulder, W.F. Stickle, P.E. Sobol, K.D. Bomben, in: J. Chastain (Ed.), Handbook of X-Ray Photoelectron Spectroscopy, Perkin-Elmer, Eden Prairie MN, 1992.
[38] Parala H, Devi A, Hipler F, Maile E, Birkner A, Becker HW, Fischer RA , J. Cryst. Growth **231**, 68 (2001).
[39] T. N. Bhat, M. K. Rajpalke, B. Roul, M. Kumar, S. B. Krupanidhi, N. Sinha, Phys. Status Solidi B, 1–4 (2011).
[40] Baba Y., Sasaki T.A., Surf. Interface Anal. **6**, 171 (1984).
[41] I. J. Lee, J. Y. Kim, H. J. Shin, and H. K. Kim, J. Appl. Phys. **95**, 5540 (2004).
[42] B.R.Natarajan, A.H. Eltoukhy, J.E. Greene, Thin Solid Films **69**, 217 (1980)

[43] Negrila, C.C., Logofatu, C., Ghita, R.V., Cotirlan, C., Ungureanu, F., Manea, A.S., Lazarescu, M.F., J. Cryst.Growth **310**, 1576 (2008).
[44] M. Faur, M. Faur, D. T. Jayne, M. Goradia, and C. Goradia, Surf. Interface Anal. **15**, 641 (1990).
[45] Hu, H.; Zhu, C.; Lu, Y. F.; Li, M. F.; Cho, B. J. *IEEE Electron Device Lett.*, **23**, 5142002
[46] Lester R. Morss, Paul P. Day, Claudia Felinto, Hermi Brito**,** J. Chem. Thermodynamics **25**(3), 415 (1993).
[47] E.H.P. Cordfunke, R.J.M. Konings, W. Ouweltjes**,** J. Chem. Thermodynamics **23**(5), 451 (1991).
[48] K. M. Yu, Z. Liliental-Weber, W. Walukiewicz, W. Shan, J. W. Ager, S. X. Li, R. E. Jones, E. E. Haller, H. Lu, W. J. Schaff, Appl. Phys. Lett. **86**, 071910 (2005).
[49] L. Mancera, J.A. Rodriguguez, N. Takeuchi, J. Phys: Condens. Matter **15**, 2625 (2003).
[50] M.A. Butler, J. Appl. Phys. **48**, 1914 (1977).
[51] A. Dixit, C. Sudakar, R. Naik, G. Lawes, J. S. Thakur, E. F. McCullen, G. W. Auner, V. M. Naik, Appl. Phys. Lett. **93**, 142103 (2008)